Journal of the European Ceramic Society 22 (2002) 471–478

www.elsevier.com/locate/jeurceramsoc

Characterisation of clay sintering process using impedance spectroscopy

Xin Wang, Ping Xiao*

Materials Group, Department of Mechanical Engineering, Brunel University, Uxbridge UB8 3PH, UK

Received 17 January 2001; received in revised form 11 May 2001; accepted 20 May 2001

Abstract

Impedance measurements were made in situ while a clay compact was being fired at different temperatures. The measured impedance spectra consist of a high frequency (HF) semicircle arc and a low frequency (LF) tail. By employing an equivalent circuit of the clay compact to simulate the impedance spectra, we have obtained values for electrical properties and the parameters of constant phase elements (CPEs) corresponding to both bulk specimen and electrode effects. Both Arrhenius plot of specimen conductance and the dielectric loss curve demonstrate a phase transition occurring in the clay at a temperature between 900 and 950 °C. Such a phase transition was believed to be the formation of a liquid phase, which was also confirmed by using XRD technique and dilatometer analysis. The variation of specimen conductance as a function of time, which was obtained from isothermal impedance measurements, was found to be in agreement with the shrinkage curve. An equation relating the electrical conductance to the density of the specimen has been established, which has been verified by examining the densification of clay during sintering. Therefore, it is promising to use impedance measurements for examining the sintering of a wide range of ceramics in situ. © 2002 Published by Elsevier Science Ltd.

Keywords: Clays; Impedance spectroscopy; Phase composition; Sintering; Vitrification

1. Introduction

In situ monitoring of sintering process is extremely important for understanding the sintering mechanisms and improving the efficiency of ceramic manufacturing. Impedance spectroscopy (IS) is a relatively mature, cheap, and simple technique for non-destructive testing, which has been widely used to characterise the electrical properties of the materials and relate the changes in these electrical properties to microstructural changes occurring in the materials. Recently, growing interest has been developed in employing IS to characterise the microstructure of ceramic materials,[1–3] particularly for studying the microstructure evolution in cement during hydration and hardening.[4–6]

In impedance measurements, a sinusoidal potential variation is applied to the test electrodes sandwiching with a specimen. Impedance Z ($=V/I$) is obtained by measuring the magnitude and phase shift of the resulting current over a range of frequency of the AC power supply. Impedance diagrams are normally expressed as Nyquist and Bode plots. The Nyquist plot shows the imaginary part of the impedance versus the real part of the impedance. The Bode plot shows the impedance as function of frequency and phase angle.

The purpose of this work is to use impedance measurements as a non-destructive approach for characterising the real-time sintering process of clay-based ceramics. Clay-based ceramics have a wide range of applications and they are the most complex ceramic materials.[7] Liquid phase sintering is the dominant mechanism in the sintering of clay based ceramics.[8] The formation of liquid phase is the crucial step in the process at which the fluidity of liquid initiates compact shrinkage. The quantity and the viscosity of liquid phase are the two important factors that determine the kinetics of sintering.[8,9] Liquid phase formed in ceramic compact at high temperature is an ionic conductor and thus acts as an electrolyte.[10] The microstructural parameters, such as the quantity of liquid phase, the porosity content and the distribution of different phases as well as the chemical composition of liquid phase would

* Corresponding author. Present address: Manchester Materials Science Centre, University of Manchester, Grosvenor Street, Manchester M1 7HS, UK.

0955-2219/02/$ - see front matter © 2002 Published by Elsevier Science Ltd.
PII: S0955-2219(01)00335-1

affect sintering process and these parameters would also keep changing as sintering proceeds. Monitoring sintering of clay-based ceramics using impedance spectroscopy will provide important information on sintering phenomena in clay.

2. Experimental procedure

2.1. High temperature measurement rig

A rig for impedance measurements at high temperature was built as shown in Fig. 1. In the rig, a wire spring was used to apply a constant pressure of about 5 N to the specimen to ensure an intimate contact between electrodes and the specimen. The electrodes were two platinum foils bonded to Al_2O_3 plates and connected to the impedance analyser. Since the resistance of the leads connecting the electrodes to the impedance analyser is much smaller than that of tested samples, the influence of the leads on impedance measurements is negligible.

2.2. Sample preparation, density measurements and phase characterisation

Ball clay (Dorset, HYMOD PRE) was ball-milled in dry mode for 5 h to produce powder of uniform particle size. The chemical composition and particle size distribution specified by the powder supplier are given in Tables 1 and 2, respectively. Pellets of 13 mm in diameter and 3–4 mm in thickness were prepared by uniaxial pressing using a pressure of 120 MPa.

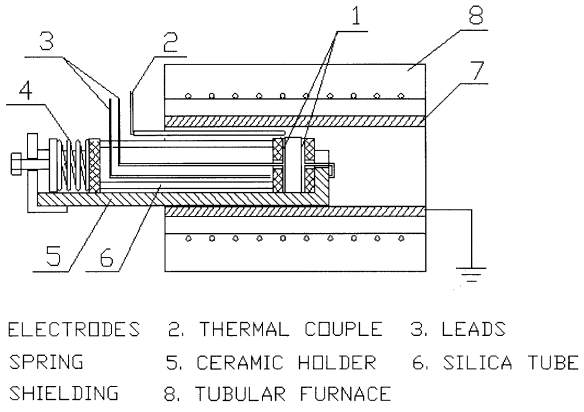

Fig. 1. Special rig for impedance measurement at high temperature.

Table 1
Chemical composition of ball clay (wt.%)

SiO_2	Al_2O_3	Fe_2O_3	TiO_2	CaO	MgO	K_2O	Na_2O	L.O.I[a]	C
54	30	1.4	1.3	0.3	0.4	3.1	0.5	8.8	0.3

[a] L.O.I.: Loss of ignition

Table 2
Particle size distribution of ball clay (wt.%)

<5 μm	<2 μm	<1 μm	<0.5 μm
96	88	79	67

Before sintering the clay, green compacts were carefully polished with SiC paper to ensure every sample was in same geometric shape. The density of the samples after sintering was determined by measuring the weight and volume of the samples. X-ray diffraction (XRD) (Philips PW1050, CuK_α radiation) was performed for phase characterisation. Dilatometer measurements were conducted using dilatometer 402 (Netzsch-Geratebau GmbH). Microstructural examination of sintered samples was carried out using SEM coupled with EDS (Jeol JXA840).

2.3. Impedance measurements

A Solartron SI 1255 HF frequency response analyser coupled with a 1296 Dielectric Interface (Solartron, UK) was used for impedance measurement. Data acquisition was undertaken using a PC computer in real time while the clay compact was being fired at different temperatures. Measurements were taken over a frequency range of 10^6 to 0.1 Hz using 1 V applied voltage with 3–6 readings per decade of frequency. Measurements with voltage lower than 0.2 V resulted in unstable response due to the high impedance of the tested sample, while measurements with voltage 0.2–3 V gave stable signal and reproducible results. Therefore, the voltage of 1 V was chosen for all impedance measurements. Measurements at a frequency of 10^6 Hz were made to determine the dielectric loss at different temperatures. Impedance spectra were analysed using the software package 'Zview for Windows' (Scribner Associates).

3. Results and discussion

3.1. Impedance spectra

Isothermal impedance measurements were made at different temperatures during firing of the clay compact. The impedance spectra measured at temperatures above 500 °C are reproducible. But at temperatures below 500 °C, several factors could affect impedance measurements, e.g. incomplete contact between sample and electrode, short circuit through a less resistive path in clay, and the presence of moisture in clay. Fig. 2 shows the Nyquist plots from impedance measurements at 700, 800, 900 and 1000 °C. There is a high frequency (HF) semicircular arc and a low frequency (LF) tail in each of

the Nyquist plots. Both the HF arc and the LF tail become smaller with increasing temperature and the cut-off frequency between HF arc and LF tail increases from 4.6 Hz at 700 °C to 4600 Hz at 1000 °C. Measurements made by using samples with varying thickness showed that the thickness of the sample affected the HF arc radii and cut-off frequency in the Nyquist plot, but had little effect on the LF tail. Therefore the HF arc can be attributed to bulk effect and the LF tail to the effect of electrode.

Normally the impedance spectrum of a polycrystalline ceramic material is expected to have two semicircular arcs, one attributed from grain and another from grain boundary. Both arcs can be examined by using a brick layer model equivalent to the structure of the polycrystalline ceramic.[1,3,11] However, there is only one semicircle attributed from clay based on the impedance measurements of the clay under firing (Fig. 2a and b). This is reasonable since a continuous network of glass phase is present in the clay at high temperatures (>950 °C). The charge carriers can transport along the network without experiencing significant blocking effect. Therefore, there is usually only one semicircle in the impedance spectra of glass samples. Such phenomena were also found in the glass containing crystallised particles and pores.[12,13] At relatively low temperature before the glass network was formed, there was still only one semicircle corresponding to the bulk effect according to the impedance spectra of the clay. This may be due to the fast electrical conduction along the particle surface. The clay minerals consist of hydrated aluminum silicates that are fine-grained and usually have a platy habit where positive ions can fit on the surface of the particles or between different layers.[14] The fine microstructure leads to a large free surface area while the mobile ions at the surface should make a major contribution to the electrical conduction in the clay at relatively high temperature (600–950 °C in this study). The materials with high porosity, if exhibiting considerable particle surface conduction, normally do not show resolved grain and grain boundary effects in their impedance spectra, because the conduction path along particle surface is a fast path. This assumption is similar to the case shown in the ionic-type humidity sensors. In the sensors, the proton hopping between neighbouring water molecules on particle surface is the dominant conduction mechanism.[15] Impedance measurements show that there was only one semicircle corresponding to the sensors.[16,17] Therefore, we believe that the semicircle from our measurements was from the bulk effect of clay.

A spike or a tail corresponding to the electrode/clay interface is always present in impedance spectra at low frequency and is assumed as electrode effect. The electrode effect was frequently encountered in the impedance measurements of cement paste,[4–6] humidity sensors,[16,17] and other ionic conducting materials.[3] The simulation of measured impedance spectra shown in the following section further confirms that the tails in impedance spectra correspond to the electrode effect.

3.2. Simulation of impedance spectra using equivalent circuit model

An equivalent circuit (Fig. 3) consisting of resistor (R) and constant phase elements (CPEs) was used to simulate the measured impedance spectra. Here CPEs were used to represent the electrical response of complex materials with a range of relaxation frequencies. The impedance of the CPE is given by:

$$Z_{\mathrm{CPE}}(j\omega) = A^{-1}(j\omega)^{-n} \tag{1}$$

Where A is a constant that is independent of frequency, ω is angular frequency and $j = \sqrt{-1}$. When

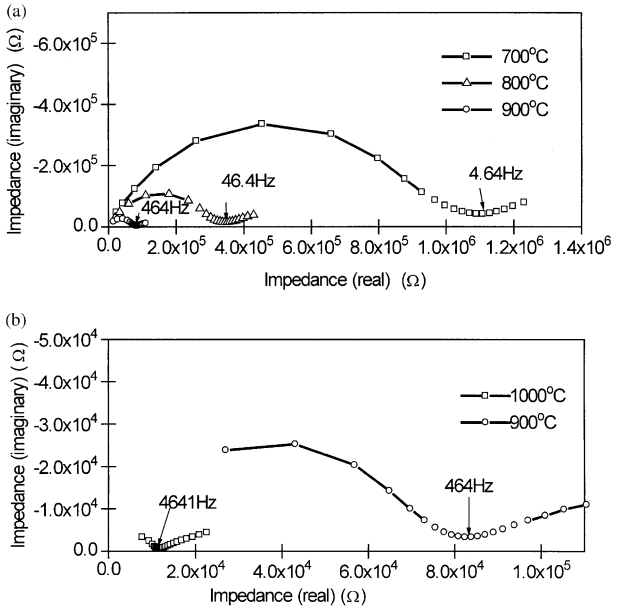

Fig. 2. (a) Nyquist plots of the clay compact at 600, 700 and 800 °C. (b) Nyquist plots of the clay compact at 900 and 1000 °C.

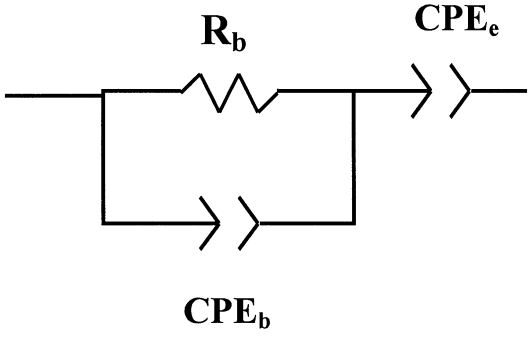

Fig. 3. Equivalent circuit of a clay compact for simulation of impedance spectra.

Table 3
Results of simulation using equivalent circuit

Temperature (°C)	R_b (ohm)	A_b (ohm^{1-n}●F^{-n})	n_b	A_e (ohm^{1-n}●F^{-n})	n_e
700	1.04×10^{6}	1.99×10^{-10}	0.730	–	–
800	3.20×10^{5}	2.70×10^{-10}	0.730	–	–
900	7.60×10^{4}	3.57×10^{-10}	0.740	2.55×10^{-5}	0.157
1000	7.83×10^{3}	4.50×10^{-10}	0.746	7.79×10^{-5}	0.250
1100	2.20×10^{3}	9.90×10^{-10}	0.768	1.04×10^{-4}	0.274

$n=1$, the CPE represents an ideal capacitor; when $n=0$, the CPE acts as a pure resistor.[18] Thus, a CPE can represent a wide variety of non-ideal elements.

This equivalent circuit model resulted in a very good fitting to the measured impedance spectra. The fitting results shown in Table 3 indicate that the resistance of the specimens decreases with increasing temperature while the parameters for CPEs increase with increasing temperature. A_e (for the electrode effect) is about five orders of magnitude larger than A_b (for the specimen). The parameter A is proportional to the capacitive effect, provided that the exponent n is not zero. The capacitance is reciprocal to the thickness of the dielectric material. Since the thickness of the electrode/clay interface is considerably smaller than that of the bulk sample. Therefore, the large A_e value further confirms that the CPE_e represents the electrode.

According to Table 3, n_b (CPE exponential index for the specimen) is much closer to 1 than n_e (CPE exponential index of the electrodes). This indicates that the CPE_e in Fig. 3 assigned for electrode effect is far from being an ideal capacitor. For a perfect flat blocking electrode, electrode effect is expected to be purely capacitive[19,20] But under our experimental condition, the contact between the clay compact and platinum electrode is poor and the electrode/clay interface is rough. It is well established that porosity of specimen or roughness of the electrode surface could lead to a frequency dispersion of the interfacial impedance and produce a constant phase angle,[19,20] which induced a spike or a tail-like plot in low frequency domain. The n_e obtained here is only 0.157–0.274, which implies an extremely high roughness at the electrode/clay interface.

The dielectric constant of the bulk specimen can be obtained by employing an equation developed by Christensen et al.:[6]

$$\varepsilon = \left(2\pi f_{top}\right)^{(2\theta/\pi-1)} 1/RA_s\varepsilon_0 \quad (2)$$

where f_{top} is the frequency at the top of the impedance arc corresponding to the specimen, θ is the depression angle, R is the resistance, $1\text{-}2\theta/\pi$ is equal to the n value in Eq. (1) and $1/A_s$ represents the geometrical factor of sample. The dielectric constants of the clay compact at 700–900 °C were calculated as 400–500. At the temperatures above 900 °C, the frequency at the top point of the bulk arc is out of the measurement range. Therefore dielectric constant cannot be calculated using Eq. (2). The dielectric constant of 400–500 is unusually high, which can only be explained by an underlying "dielectric amplification factor" (DAF) mechanism. DAF usually results from a microstructural arrangement where isolated conductive domains imbed in a continuous insulating matrix. This factor is responsible for the large effective dielectric constants of a barrier layer capacitor, where conductive grains are surrounded by insulating grain boundary.[6] DAF was also found to exist in cements where a conductive pore solution is separated by insulating product C–S–H layer[4,5] and in Al_2O_3/SiC nano-composite where conductive SiC particles imbedded in Al_2O_3 matrix result in larger capacitance.[19] Further work is needed to clarify what is responsible for DAF in clay compact at high temperature.

3.3. The sensitivity of impedance measurements to the formation of liquid phase

Fig. 2b shows an incomplete bulk semicircles which loses high frequency part when the measurements were made at 900 and 1000 °C, where the relaxation frequency of the clay at 1000 °C was well above 1 MHz. This suggests that the clay behaved like a conducting electrolyte at 1000 °C, which may be due to the formation of a continuous conductive liquid phase in the clay compact. Fig. 4 shows an Arrhenius plot based on the

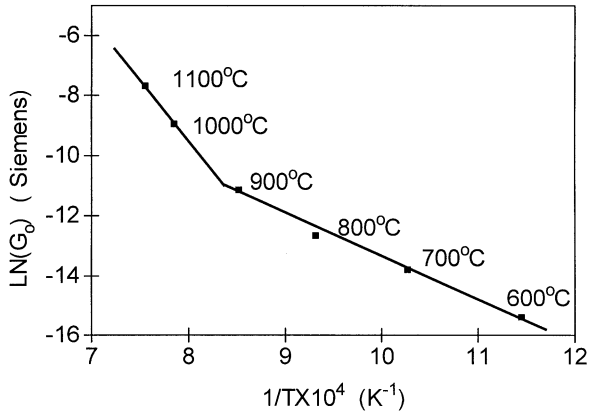

Fig. 4. Arrhenius plot of bulk conductance as a function of temperature.

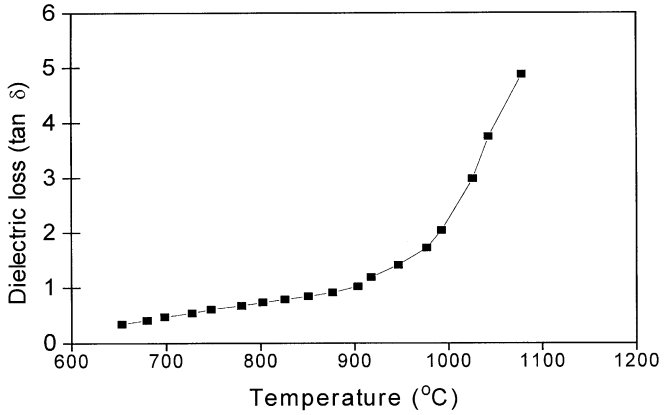

Fig. 5. Loss tangent (at 1 MHz) obtained from impedance measurement as a function of temperature.

data in Table 3, which suggests different activation energy in different temperature range. Obviously there is a bend at about 920 °C, which indicates that the conducting mechanism in the clay changes when the temperature exceeds 920 °C. Meanwhile, based on impedance spectra, the dielectric loss factor (at 1 MHz) in the clay compact (Fig. 5) also shows a significant increase at temperature above 900 °C.

The XRD analysis after heat treatment at 850 and 900 °C shows that no apparent phase transformation occurred, whereas after heat treatment at 950 °C the amount of kaolinite and mica seems to decrease (Fig. 6). The heat treatment at 1020 °C lead to nearly complete disappearance of kaolinite and mica. Meanwhile, the phase transformation in the clay also involved the disappearance and formation of glassy phases, which cannot be identified using XRD. It is believed that the diminishing mica and kaolinite in clay compact is related to the formation of a liquid phase.[22–25] Therefore, the XRD analysis suggests the presence of the liquid phase in clay at temperature between 900 and 950 °C.

The dominant mechanism in the sintering of clay-based ceramics is vitrification where significant shrinkage can not occur unless a certain amount of liquid phase is present.[8,9] The shrinkage curve (Fig. 7) measured using dilatometer further confirms that the liquid phase was formed at temperature around 950 °C, where significant shrinkage occurred above 950 °C. The liquid phase formation led to a significant change in bulk conductance and dielectric loss curve at temperatures around 950 °C.

d.c. Electrical conductivity measurements have already been used to detect the presence of liquid phase in the Al_2O_3–1 mol% TiO_2–0.5 mol% $NaO_{1/2}$ system.[10] The electrical measurements were found to be sensitive to the presence of a small amount of liquid phase that may influence or control the sintering of many ceramic compositions. Impedance spectroscopy is a much more sophisticated technique than the d.c. conductivity

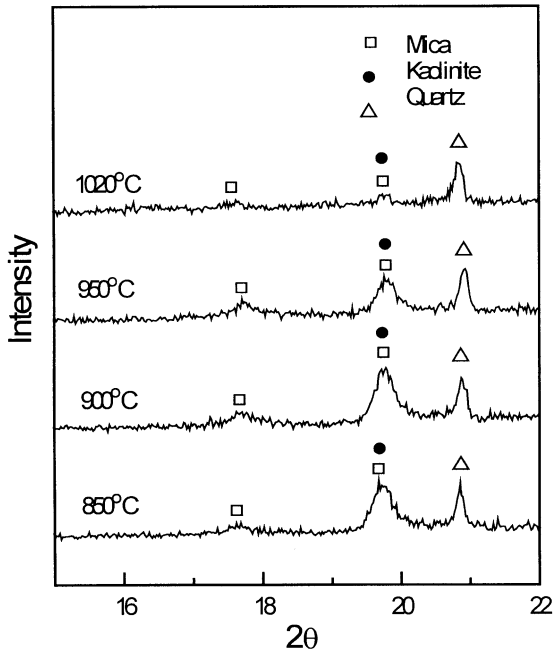

Fig. 6. XRD patterns of the clay compacts after 20 min sintering at different temperature.

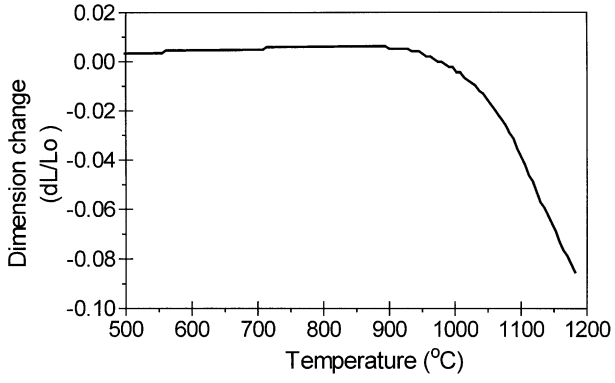

Fig. 7. Shrinkage curve of a clay compact measured using a dilatometer with the heating rate was 5 °C/min.

measurement technique. More information, e.g. capacitative effects, dielectric loss and electrode polarisation, etc. can be obtained from impedance spectra. The electrode effect can be excluded for examining the electrical properties of the specimen only. In this work, the formation of liquid phase during firing was not only detected by the change in the activation energy for electrical conduction, but also determined by an abrupt increase in the dielectric loss (Fig. 4). Therefore, impedance measurements are more effective in detecting the presence of liquid phase during sintering of ceramics.

3.4. Monitoring the densification process

To monitor the densification process of clay, impedance measurements at different time intervals have been made at various temperatures. Impedance measurements at 800 °C showed little change in measured impedance spectra (Fig. 8a), whereas the impedance spectra measured at temperatures above 950 °C (Fig. 8b–d) showed a gradual shift towards the left. However, spectra parameters, i.e. the dielectric loss, the cut-off frequency and the length of LF tail, etc. remained almost unchanged with sintering time. This indicated that the densification occurred at temperatures above 950 °C, where little change in the composition occurred during sintering at this temperature. Fig. 8b–d shows the multiple impedance spectra of the clay at 1050, 1100 and 1150 °C, respectively. The spectra shifted quickly at the initial stage of sintering and slowly at the later stage of sintering. In addition, the spectra shifted faster with increasing sintering temperature. This trend of spectrum shifting is in agreement with the sintering behaviour of ceramics where the densification rate is higher at higher temperature and it slows down when shrinkage curve approaches an asymptote.

As is well established, the diameter of a semicircle in impedance spectrum is representative of the resistance.[1–3,21] The semicircle corresponding to the bulk specimen is clearly distinguished from the spectra corresponding to the electrode effect (Fig. 8b–d). The diameter of the semicircle can be taken as the real part at the cut-off frequency. By neglecting the resistance of leads that is lower than 0.1% of the resistance of bulk clay, then the diameter of the semicircle can be taken as the bulk resistance. The electrical resistance can be described as:

$$R = \delta/\sigma \cdot A_e \tag{3}$$

where σ is the conductivity, δ is the distance between electrodes and A_e is the area of electrodes. During impedance measurements, the parameter A_e can be considered as a constant, but both σ and δ changed due to densification of the clay compact. Therefore, both increasing electrical conductivity and decreasing distance between electrodes contribute to the decreasing the resistance of the specimen.

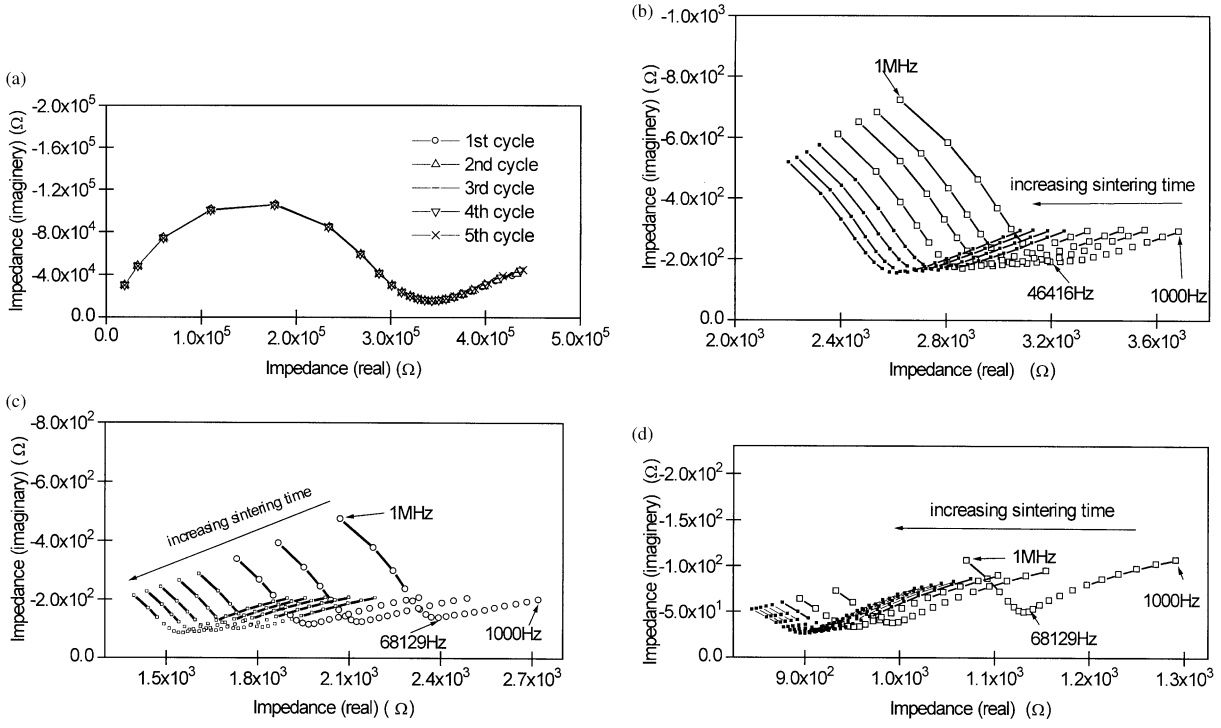

Fig. 8. Multiple impedance measurements at time intervals of 5 min, each measurement taking 2.62 min: (a) at 800 °C; (b) at 1050 °C; (c) at 1100 °C; (d) at 1150 °C.

According to SEM observation and XRD analysis, the sintered clay compact mainly contains a continuous glass phase and isolated pores where the quartz and mullite particles are imbedded in glass phase. To analyse the electrical conductivity of the clay, we can treat this material as a two-phase composite. The continuous glass phase containing crystal particles is treated as one single conducting phase while the isolated pores can be regarded as another insulating phase. The structure of the clay is very similar to the 3–0 connectivity pattern shown in piezoelectric–pyroelectric composites studied previously.[26] When the conductivity of the insulating phase, e.g. pores, is zero, the electrical conductivity of the composite can be estimated using the equation:[27]

$$\sigma_m = \sigma_h(1-f)^m \tag{4}$$

where σ_m is the electrical conductivity of the composite, σ_h is the electrical conductivity of continuous conductive network in the composite, f is the fraction of the insulating phase and the m here is an exponent representing the particle shape and distribution.[27]

Another equation for calculating the transport properties of porous materials has been developed as[28,29]

$$\Phi^c/\Phi_m = f_{\alpha c} \tag{5}$$

where Φ^c refers to the transport properties of a porous material, Φ_m refers to the transport properties of matrix without porosity and $f_{\alpha c}$ is a topological parameter. The topological parameter $f_{\alpha c}$ depends not only on the volume fraction of matrix phase, but also on the microstructure parameters, such as pore size, pore shape and pore distribution. In general, it can be assumed to follow the power law:[26,27]

$$f_{\alpha c} = f_\alpha^m \tag{6}$$

where f_α is the volume fraction of matrix, the m here is a parameter which is dependent on several microstructural parameters as mentioned above. Combining Eqs. (5) and (6), we have:

$$\Phi^c = \Phi_m f_\alpha^m \tag{7}$$

It is obvious that Eq. (7) is the same as Eq. (4).

In Eq. (7), f_α is equal to the ratio (D_b/D_t) of actual bulk density (D_b) to the theoretical density (D_t) of the sample. Therefore, by combining Eqs. (3) and (7), we express the electrical conductance (G) in terms of the density, D_b and the thickness of the specimen, δ:

$$G = 1/R = C \cdot D_b^m/\delta \tag{8}$$

where $C = A_e \cdot \sigma_m/D_t^m$, which can be assumed to be constant during sintering at a certain temperature.

Based on the impedance spectra measured at 1100 °C (Fig. 8c), the conductance G of the bulk sample under firing was obtained as a function of sintering time (Fig. 9a). The density and dimension change of sample were measured after quenching the samples, which were being sintered at 1100 °C (Fig. 9b–c). Clearly, the three plots shows similar trend.

By using the data of D_b and δ shown in Fig. 9b–c and assuming $m = 2$, we calculated the conductance of the sample according to Eq. (6) (in Fig. 9a). The change of conductance was displayed in Fig. 9 showing that calculated data of the conductance fits the measured curve from the impedance measurements very well. It is interesting to note that the assumption of m as a constant of 2 gives a very good fitting to the experimental results, while m is dependent on the microstructural parameters, e.g. pore shape and pore distribution.

The value of m was often found to be in the range of 1.65 to 2.0,[27] so $m = 2$ in this work is quite reasonable. When $m = 3-5$, it imply the extreme geometries or complex structures of the dispersing phase.[30] In the clay during sintering where the continuous phase is glass phase and the material is quite pliable, pores are more likely to have similar shapes and well distributed. This might be the reason why m remains as constant during the densification process.

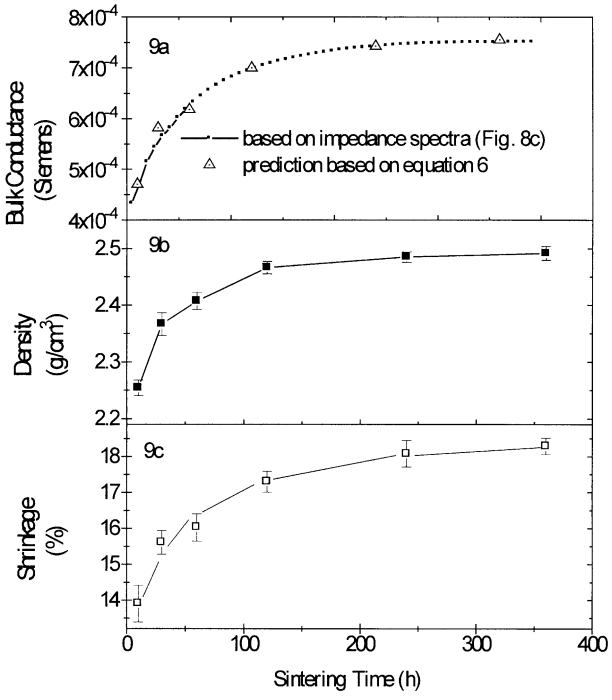

Fig. 9. (a) Bulk conductance versus sintering time, where the dotted line was obtained from impedance measurements; the triangles were calculated using Eq. (6); (b) and (c) the density and dimension change of the clay during sintering at 1100 °C. Each value was obtained from the average value from the measurements of five samples.

4. Conclusion

Impedance measurements of clay compact under firing were conducted in situ at high temperatures. The effect of bulk sample is well distinguished from the electrode effect. The electrical properties, such as conductance, loss tangent and dielectric constant of bulk sample can be obtained from impedance spectra using equivalent circuit model simulation. The variations of electrical conductance and loss tangent of bulk sample versus temperature are indicative of the formation of liquid phase during sintering. The variation electrical conductance of bulk compact versus sintering time can be used to monitor the real time densification process of clay compact under firing. Impedance spectroscopy is believed to be a promising tool for investigating the sintering process of liquid-phase sintering ceramics.

References

1. Muccillo, E. N. S. and Kleitz, M., Impedance spectroscopy of Mg-partially stabilised zirconia and cubic phase decomposition. *J. Eur. Ceram. Soc.,* 1996, **16**, 453–465.
2. Rodrigues, C. M. S., Labrincha, J. A. and Marques, F. M. B., Monitoring of the corrosion of YSZ by impedance spectroscopy. *J. Eur. Ceram. Soc.,* 1998, **18**, 95–104.
3. Steil, M. C., Thevenot, F. and Kleitz, M., Densification of yttria-stabilised zirconia-impedance spectroscopy analysis. *J. Electrochem. Soc.,* 1997, **1**, 390–398.
4. McCarter, W. J., Garvin, S. and Bouzid, N., Impedance measurement on cement paste. *J. Mater. Sci. Lett*., 1988, 1056–1057.
5. Christensen, B. J., Mason, T. O. and Jennings, H. M., Influence of silica fume on the early hydration of portland cements using impedance spectroscopy. *J. Am. Ceram. Soc.,* 1992, **75**, 939–945.
6. Christensen, B. J., Coverdale, R. T., Olseon, R. A., Ford, S. J., Carboczi, E. J., Jennings, H. M. and Mason, T. O., Impedance spectroscopy of hydrating cement-based materials: measurement, interpretation, and application. *J. Am. Ceram. Soc.,* 1994, **77**, 2789–2804.
7. Carty, W. M. and Senapati, U., Porcelain-raw materials, processing, phase evaluations, and mechanical behaviour. *J. Am. Ceram. Soc.,* 1998, **81**, 3–20.
8. Kingery, W. D., Bowen, K. K. and Uhlmann, D. R., Grain growth, sintering and vitrification. In *Introduction to Ceramics,* 2nd edn, ed. E. Burke, B. Chalmers and J. A. Krumhansl. John Wiley & Sons, New York, 1976 pp. 448–575.
9. Anseau, M. R., Deletter, M. and Cambier, F., The separation of sintering mechanisms for clay-based ceramics. *Trans. J. Br. Ceram. Soc.,* 1981, **80**, 142–146.
10. Morgan, P. E. D. and Koutsoutis, M. S., Electrical conductivity measurements to detect suspected liquid phase in the Al_2O_3–1 mol% TiO_2–0.5 mol% $NaO_{1/2}$ and other systems. *J. Am. Ceram. Soc.,* 1986, **67**, c254–c255.
11. Bauerle, J. E., Study of solid electrolyte polarisation by a complex admittance method. *J. Phys. Chem. Solids,* 1969, **30**, 2657.
12. Murugan, G. S. and Varma, K. B. R., Characterisation of lithium borate-bismuth tungstate glasses and glass-ceramics by impedance spectroscopy. *Solid State Ionics,* 2001, **239**, 105–112.
13. Abrahams, I. and Hadzifejzovic, E., Lithium ion conductivity and thermal behaviour of glasses and crystallised glasses in the system Li_2O–Al_2O_3–TiO_2–P_2O_5. *Solid State Ionics,* 2000, **134**, 249–257.
14. Kingery, W. D., Bowen, H. K. and Uhlmann, D. R., Structure of Crystals. In *Introduction to Ceramics,* 2nd edn, ed. E. Burke, B. Chalmers and J. A. Krumhansl. John Wiley & Sons, New York, 1976, pp. 77.
15. Traversa, E., Ceramic sensors for humidity detection: the state-of-the-art and future developments. *Sensors and Actuators B,* 1995, **23**, 135–156.
16. Hwang, J.-H., Mason, T. O., Buehler, M. F., Darab, J. G., Matson, D. W. and Linehan, J. C., Characterisation of humidity-sensing NiO-$Ni(OH)_2$ nanocomposites by impedance spectroscopy. *Mater. Sci. Eng.,* 1995, **A204**, 252–257.
17. Gusmano, G., Bianco, A., Montesperlli, G. and Traversa, E., An EIS study of the humidity-sensitive electrical conduction of alkali-doped TiO_2 films. *Electrochemica. Acta,* 1996, **41**, 1359–1368.
18. Amaral, S. T. and Muller, I. K., Effect of silicate on passive films anodically formed on iron in alkaline solution as studied by electrochemical impedance spectroscopy. *Corrosion,* 1999, **55**, 19–23.
19. Armstrong, R. D. and Todd, M., Interfacial electrochemistry. In *Solid State Electrochemistry*, ed. P. G. Bruce. Cambridge University Press, Cambridge, 1995, pp. 264–291.
20. Raistrick, I. D., Current distribution, porous, and rough electrodes—the effect of geometry. In *Impedance Spectroscopy*. ed. J. Ross Macdonald. John Wiley & Sons, New York, 1987, pp. 78–84.
21. Wang, X. and Xiao, P., Non-destructive characterisation of alumia/silicon carbide nanocomposites using impedance spectroscopy. *J. Eur. Ceram. Soc.,* 2000, **20**, 2591–2599.
22. Shuller, K. H., Reaction between mullite and glassy phase in porcelains. *Trans. Br. Ceram. Soc.,* 1964, **63**, 102–107.
23. Sarikaya, S. M. and Aksay, I. A., Spinel phase formation during 980c exothermic reaction in the kaolin-mullite reaction series. *J. Am. Ceram. Soc.,* 1987, **70**(11), 837–842.
24. Okada, K., Otsuka, N. and Ossaka, J., Characterisation of spinel phase formed in the kaolin-mullite thermal sequence. *J. Am. Ceram. Soc.,* 1986, **69**(10), c251–c253.
25. Lundin, S. T., Microstructure of porcelain. In *Microstructure of Ceramic Materials*. NBS Misc. Publ., 1964, 257, 93–106.
26. Newnham, R. E., Skinner, D. P. and Cross, L. E., Connectivity and piezoelectric-pyroelectric composites. *Mater. Res. Bull.,* 1978, **13**, 525–536.
27. Mclachlan, D. S., Blaszkiewicz, M. and Newnham, R. E., Electrical resistivity of composites. *J. Am. Ceram. Soc.,* 1990, **73**(8), 2187–2203.
28. Fan, Z., A microstructural, approach to the effective transport properties of multiphase composites. *Philos. Mag. A,* 1996, **73**, 1663–1684.
29. Fan, Z., Tsakiropoulos, P. and Miodownik, A. P., Prediction of Young's modulus of particulate two phase composites. *Mater. Sci. Technol.,* 1992, **8**, 922–929.
30. Balberg, I., Tunneling and nonuniversal conductivity in composites materials. *Phys. Rev. Lett.,* 1987, **59**, 1305–1308.